

AperTO - Archivio Istituzionale Open Access dell'Università di Torino

A generalized ratiometric chemical exchange saturation transfer (CEST) MRI approach for mapping renal pH using iopamidol

This is the author's manuscript

Original Citation:

Availability:

This version is available <http://hdl.handle.net/2318/1716640> since 2019-11-20T16:44:02Z

Published version:

DOI:10.1002/mrm.26817

Terms of use:

Open Access

Anyone can freely access the full text of works made available as "Open Access". Works made available under a Creative Commons license can be used according to the terms and conditions of said license. Use of all other works requires consent of the right holder (author or publisher) if not exempted from copyright protection by the applicable law.

(Article begins on next page)



A Generalized Ratiometric Chemical Exchange Saturation Transfer (CEST) MRI Approach for Mapping Renal pH using Iopamidol

Journal:	<i>Magnetic Resonance in Medicine</i>
Manuscript ID	Draft
Wiley - Manuscript type:	Note
Date Submitted by the Author:	n/a
Complete List of Authors:	Wu, Yin; Paul C. Lauterbur Research Centre for Biomedical Imaging, Institute of Biomedical and Health Engineering, Shenzhen Institutes of Advanced Technology, Chinese Academy of Sciences; Key Laboratory of Health Informatics, Chinese Academy of Sciences Zhou, Iris; Massachusetts General Hospital, Martinos Center; Harvard Medical School, Igarashi, Takahiro; Massachusetts General Hospital, Martinos Center Longo, Dario; CNR, Institute of Biostructure and Bioimaging; Molecular Imaging Center, Molecular Biotechnology and Health Sciences Aime, Silvio; University of Turin, Chemistry IFM Sun, Phillip; Harvard Medical School, Radiology
Research Type:	Contrast agents < Contrast < Biophysics < Technical Research, Magnetization transfer < Technique Development < Technical Research
Research Focus:	Other tissues (body fluids, skin, vessels, arteries, other organs, etc)

SCHOLARONE™
Manuscripts

1
2 **A Generalized Ratiometric Chemical Exchange Saturation Transfer (CEST) MRI Approach for**
3
4 **Mapping Renal pH using Iopamidol**
5
6
7

8 Yin Wu,^{1,2} Iris Y. Zhou,¹ Takahiro Igarashi,¹ Dario L. Longo,³ Silvio Aime,⁴ and Phillip Zhe Sun^{1*}
9
10

11
12 ¹ Athinoula A. Martinos Center for Biomedical Imaging, Department of Radiology, Massachusetts
13 General Hospital and Harvard Medical School, Charlestown, MA 02129, USA
14

15
16 ² Paul C. Lauterbur Research Centre for Biomedical Imaging, Shenzhen Key Laboratory for MRI,
17 Shenzhen Institutes of Advanced Technology, Chinese Academy of Sciences, Shenzhen, Guangdong
18
19 518055, China
20
21

22
23 ³ Institute of Biostructure and Bioimaging (CNR) c/o Molecular Biotechnology Center, University of
24
25 Torino, Torino, Italy
26
27

28
29 ⁴ Department of Molecular Biotechnology and Health Sciences, Molecular Imaging Center, University of
30
31 Torino, Torino, Italy
32
33
34
35

36 **Correspondence Author:**
37

38
39 Phillip Zhe Sun, PhD (pzhesun@mgh.harvard.edu)
40

41 Athinoula A. Martinos Center for Biomedical Imaging
42

43 Massachusetts General Hospital and Harvard Medical School
44

45 Charlestown, MA 02129, USA
46

47 Phone: (1) 617-726-4060; Fax: (1) 617-726-7422
48
49

50
51 **Word Counts: 2,375**
52
53

54
55 **Running title: Generalized Ratiometric CEST renal pH imaging**
56
57
58
59
60

ABSTRACT

Purpose

To extend the pH detection range of iopamidol-based ratiometric chemical exchange saturation transfer (CEST) MRI at sub-high magnetic field and establish quantitative renal pH MRI.

Methods

CEST imaging was performed on iopamidol phantoms with pH of 5.5-8.0 and in vivo on rat kidneys (N = 5) during iopamidol administration at a 4.7 Tesla. Iopamidol CEST effects were described using a multi-pool Lorentzian model. A generalized ratiometric analysis was conducted by ratioing resolved iopamidol CEST effects at 4.3 and 5.5 ppm obtained under 1.0 and 2.0 μT , respectively. The pH detection range was established for both the conventional ratiometric analysis and the proposed approach. Renal pH was mapped in vivo with regional pH assessed by one-way ANOVA.

Results

Good fitting performance was observed in multi-pool Lorentzian decoupling of CEST effects, both in the iopamidol phantom and rat kidneys ($R^2\text{s} > 0.99$). The proposed approach extends the in vitro pH detection range to 5.5-7.5 at 4.7 Tesla. In vivo renal pH was measured to be 7.0 ± 0.1 , 6.8 ± 0.1 and 6.5 ± 0.2 for cortex, medulla and calyx, respectively ($P < 0.05$).

Conclusion

The proposed ratiometric approach extended the iopamidol pH detection range, enabled renal pH mapping in vivo, promising for pH imaging studies at sub-high or low fields with potential clinical applicability.

Key words: Chemical exchange saturation transfer; ratiometric imaging, kidney, pH, iopamidol

INTRODUCTION

Magnetic resonance imaging (MRI) serves as a versatile technique to assess kidney functionality. As kidney plays a vital role in balancing body acid/base homeostasis, pH MRI is promising to identify renal dysfunction, diagnose regional kidney injury before symptom onset and ultimately, guide treatment prior to irreversible damage (1-3). However, conventional pH measurement techniques, including lactate, phosphorous and hyperpolarized ^{13}C magnetic resonance spectroscopy (MRS) are limited for routine renal imaging due to their relatively coarse spatiotemporal resolution or requirement of polarization devices (4-8). Gadolinium-based pH imaging provides novel insight of renal physiology and its disruption, yet it requires independent determination of local contrast agent concentration (9,10). Although this can be achieved by administering a second pH-insensitive agent with identical tissue pharmacokinetics, the repeated injection of contrast agents makes it somewhat cumbersome (1,11). The development of pH-sensitive PET/MRI hybrid contrast agent elegantly harnesses the pH sensitivity, MRI resolution and PET quantification of contrast agent concentration for pH mapping. However, this approach requires simultaneous PET and MRI acquisition, which is not widely available yet (12).

Iopamidol, an FDA-approved computed tomography contrast agent, has two distinct MR visible chemical exchangeable groups of different pH-dependent exchange rate. The development of ratiometric chemical exchange saturation transfer (CEST) MRI enables concentration-independent pH imaging (13-15). Its pH detection range has been shown to be 5.5-7.4 at 7 Tesla (T) and 6.0-7.6 at 14 T (16,17). Additional CEST agents have been investigated for pH imaging, including iopromide (18), imidazoles (19), and paramagnetic CEST (paraCEST) agents (20). Recently, radio-frequency (RF) power-based ratiometric pH MRI has been proposed that enables ratiometric MRI using iobitridol, a CEST agent with a single exchangeable group, for renal pH imaging (21). It is worthwhile to point out that most renal pH MRI studies thus far have been demonstrated at high fields (≥ 7 Tesla). When translated to low/sub-high field, the dynamic pH range has been substantially reduced due to

1 overlapped CEST effects and more prominent concomitant saturation transfer effects (16,22). As renal
2 pH spans a relatively broad range, (1,2,16,21), our study aimed to devise a new means of ratiometric
3 CEST MRI to enable renal pH imaging at 4.7 T as a pertinent step forward toward clinical application.
4
5
6
7

8 METHODS

9 MRI studies

10 The prospective study was conducted on a 4.7 T small-bore MRI scanner (Bruker Biospec,
11 Billerica, MA). We used iopamidol phosphate buffered solution (PBS) phantom for pH calibration (16).
12 Briefly, pH of 40 mM iopamidol PBS solution was titrated to 5.5, 6.0, 6.5, 7.0, 7.5 and 8.0, and imaged
13 under 37°C. We used single-shot spin-echo (SE) echo planar imaging (EPI) with a field of view (FOV) of
14 52×52 mm², image matrix = 96×96 and slice thickness = 5 mm. We collected two Z-spectra for RF power
15 (B₁) levels of 1.0 and 2.0 μT (frequency offsets between ±7 ppm with intervals of 0.25 ppm, repetition
16 time (TR)/saturation time (TS)/echo time (TE)=10,000/5,000/48 ms). Water saturation shift
17 referencing (WASSR) map was collected with B₁=0.3 μT (frequency offsets between ±0.125 ppm with
18 intervals of 0.025 ppm, TR/TS=2,000/1,000 ms).
19
20
21
22
23
24
25
26
27
28
29
30
31
32
33
34

35 In vivo experiments have been approved by the local Institutional Animal Care and Use
36 Committee. Briefly, adult male Wistar rats (N = 5, 292± 28g) were initially anesthetized with
37 5% isoflurane. Endotracheal intubation was performed after the animal was sufficiently anesthetized.
38 The animals were mechanically ventilated at a rate of 60±2 bpm with 1.5-2% isoflurane in
39 room-temperature air using a ventilator (Kent Scientific, Torrington, CT). Their body temperature was
40 maintained at 37°C by a circulating warm water jacket positioned around the torso. A single slice
41 image along the long axis of kidney was imaged with CEST MRI during iopamidol administration (FOV=
42 20×20 mm², image matrix = 48×48, slice thickness = 4 mm). Briefly, iopamidol (Isovue200, 1.5 mg l/g
43 b.w.) was infused at a typical clinical dose via the tail vein using a syringe pump, with bolus injection
44 of half of the dose at a rate of 18 ml/hr and continuous infusion of the rest of the contrast agent at a
45 rate of 2 ml/hr during the CEST image acquisition. Respiratory gating was implemented before RF
46
47
48
49
50
51
52
53
54
55
56
57
58
59
60

1 saturation and data acquisition. WASSR map (frequency offsets between ± 0.5 ppm with intervals of
 2 0.05 ppm, $B_1=0.3 \mu\text{T}$) and two Z-spectra (frequency offsets between ± 7 ppm with intervals of 0.125
 3 ppm, $TR/TS/TE = 6,000/3,000/18$ ms) with B_1 levels of 1.0 and 2.0 μT were collected (15). The total
 4 scan time was approximately 45 min.
 5
 6
 7
 8
 9

10 Data analysis

11 Data were analyzed in MATLAB (MathWorks, Natick, MA). Z-spectra (M_z) were centered using
 12 the WASSR map and normalized by the signal without RF irradiation (M_0) (23,24). The Z-spectra were
 13 inverted as $(1-M_z/M_0)$ and decoupled using a multi-pool Lorentzian model,
 14
 15

$$16 Z(w) = \sum_{i=1}^7 L_i(w) \quad \text{Eq. (1)}$$

17 where L_i is the Lorentzian spectrum of the i^{th} pool. Saturation transfer effects, including nuclear
 18 overhauser effect (NOE), magnetization transfer (MT), direct water saturation, iopamidol CEST effects
 19 of two hydroxyl groups (-OH) and two amide groups were solved using multi-pool Lorentzian model,
 20 with their chemical shifts at -3.2, -1.5, 0, 0.8, 1.8, 4.3 and 5.5 ppm, respectively (25,26),
 21
 22

$$23 L(w) = \frac{A}{1 + 4\left(\frac{w - w_0}{lw}\right)^2} \quad \text{Eq. (2)}$$

24 where w is the frequency offset, A , w_0 , and lw are the amplitude, center frequency and linewidth of
 25 the i^{th} saturation transfer effects, respectively.
 26
 27
 28
 29
 30
 31
 32
 33

34 To minimize the bias of initial guesses, a recently developed Image Downsampling Expedited
 35 Adaptive Least-squares (IDEAL) fitting method was used (27). Briefly, CEST images were down-sampled
 36 to a single pixel to achieve high signal-to-noise ratio (SNR) for the initial fitting. Relaxed constraints
 37 were chosen, with peak and linewidth bounds between 1% and 100 times of the initial guesses, and the
 38 peak frequency shift within ± 0.2 ppm of each chemical shift. CEST images were then resampled to 2×2 ,
 39 4×4 , 8×8 , 12×12 , 24×24 till the original resolution of 48×48 , with the initial guesses of each voxel
 40 determined from the fitting results of the nearest voxel from the last down-sampled images. The
 41
 42
 43
 44
 45
 46
 47
 48
 49
 50
 51
 52
 53
 54
 55
 56
 57
 58
 59
 60

constraints were reduced to between 10% and 10 times of the iterative initial values. Nonlinear constrained fitting algorithm was used with two-fold overweighting applied for Z-spectra between 4.0 and 5.8 ppm to increase the fitting accuracy of iopamidol CEST effects at 4.3 and 5.5 ppm. Goodness of fitting (R^2) was calculated for each pixel. Ratiometric measurement was obtained by ratioing multi-Lorentzian model decoupled ST effects at 5.5 ppm obtained under B_1 of 2.0 μT to that at 4.3 ppm obtained under B_1 of 1.0 μT ,

$$R_{ST} = \frac{ST_{5.5 \text{ ppm}, 2.0 \mu\text{T}}}{ST_{4.3 \text{ ppm}, 1.0 \mu\text{T}}} \quad \text{Eq. (3)}$$

For the conventional ratiometric methods, the ST effects at chemical shifts of 4.3 and 5.5 ppm were measured with asymmetric analysis of $ST(\omega) = \frac{M(-\omega) - M(\omega)}{M_0}$, where ω is the chemical shift of iopamidol amide proton with respect to the water resonance. To calibrate ratiometric CEST effect toward absolute pH, in vitro pH calibration was obtained using a polynomial fitting of R_{ST} as a function of titrated pH (16). The standard deviation of precision (SDP) was calculated (18). Renal pH from ratiometric analysis of the same RF power level (e.g. $ST(5.5 \text{ ppm})/ST(4.3 \text{ ppm})$ under 1.0 and 2.0 μT) and mixed RF power levels (e.g. $ST(5.5 \text{ ppm}, 2.0 \mu\text{T})/ST(4.3 \text{ ppm}, 1.0 \mu\text{T})$ and $ST(5.5 \text{ ppm}, 1.0 \mu\text{T})/ST(4.3 \text{ ppm}, 2.0 \mu\text{T})$) was investigated for both of the proposed and conventional ratiometric methods (Supplementary Information). One-way analysis of variance (ANOVA) with Bonferroni correction was conducted and P values less than 0.05 were considered statistically significant.

RESULTS

Figure 1 shows two representative CEST Z-spectra from the iopamidol PBS phantom (pH=7.0) obtained under B_1 of 1.0 and 2.0 μT . There is substantial overlap between iopamidol CEST effects at 4.3 and 5.5 ppm, with 4.3 ppm signal much stronger than that of 5.5 ppm. Multi-pool Lorentzian line decoupling (Eq. 1) resolves multiple overlapping CEST effects from the Z-spectrum, allowing improved calculation of the ratiometric analysis. Note that high R^2 s >0.99 were achieved for all vials and power levels, indicating good fitting performance.

1
2
3
4 Figure 2 shows that the ratiometric analysis of decoupled CEST effects extended the range of
5 pH detection from that using the conventional ratiometric analysis. Specifically, the routine
6 ratiometric analysis (blue squares) has a narrow pH range of 5.5-7.0. This is because for pH above 7.0,
7
8 chemical exchange rate at 5.5 ppm becomes relatively fast with respect to that of 4.3 ppm, making it
9 inefficient to detect using moderate RF saturation power levels. Note that the pH detection range
10 determined in vitro (i.e. 5.5-7.0) will likely be reduced when translated in vivo due to more
11 pronounced concomitant magnetization transfer and direct saturation effects in tissue. Fortunately,
12 the modified ratiometric analysis of decoupled CEST effects extended the pH detection range to
13 5.5-7.5 (SDP = 0.12 pH unit), aiding in vivo renal pH imaging. Figure 3 shows in vitro CEST images from
14 the conventional asymmetry analysis at 5.5 ppm ($B_1=2.0 \mu\text{T}$, Fig. 3a) and at 4.3 ppm ($B_1=1.0 \mu\text{T}$, Fig.
15 3b). The conventional ratiometric image (Fig. 3c) can map pH up to 7.0 (Fig. 3d). In comparison, Figs.
16 3e and 3f show CEST images obtained from the line-decoupling approach, with the modified
17 ratiometric image shown in Fig. 3g. The modified ratiometric analysis is sensitive to pH as high as 7.5
18 (Fig. 3h), extending from the relatively narrow pH range obtainable using the conventional ratiometric
19 analysis.

20
21
22
23
24
25
26
27
28
29
30
31
32
33
34
35
36
37
38
39 Figure 4 shows inverted Z-spectra (i.e., $1-M_z/M_0$) from regions of calyx, medulla and cortex of a
40 representative rat kidney following iopamidol injection, obtained under B_1 of 1.0 μT (left column) and
41 2.0 μT (right column), fitted with a multi-pool Lorentzian model. The amplitude of CEST effect at 5.5
42 ppm decreases from calyx to cortex under B_1 of 2.0 μT , whereas the ST effect at 4.3 ppm shows
43 relatively small change under B_1 of 1.0 μT , suggesting consecutive renal pH decrease from the
44 outermost to the innermost layers. Good fitting was observed for all layers with $R^2>0.99$. We further
45 confirmed that the modified ratiometric pH imaging provides improved renal pH mapping in vivo.
46
47
48
49
50
51
52
53
54
55
56
57
58
59
60
61
62
63
64
65
66
67
68
69
70
71
72
73
74
75
76
77
78
79
80
81
82
83
84
85
86
87
88
89
90
91
92
93
94
95
96
97
98
99
100
101
102
103
104
105
106
107
108
109
110
111
112
113
114
115
116
117
118
119
120
121
122
123
124
125
126
127
128
129
130
131
132
133
134
135
136
137
138
139
140
141
142
143
144
145
146
147
148
149
150
151
152
153
154
155
156
157
158
159
160
161
162
163
164
165
166
167
168
169
170
171
172
173
174
175
176
177
178
179
180
181
182
183
184
185
186
187
188
189
190
191
192
193
194
195
196
197
198
199
200
201
202
203
204
205
206
207
208
209
210
211
212
213
214
215
216
217
218
219
220
221
222
223
224
225
226
227
228
229
230
231
232
233
234
235
236
237
238
239
240
241
242
243
244
245
246
247
248
249
250
251
252
253
254
255
256
257
258
259
260
261
262
263
264
265
266
267
268
269
270
271
272
273
274
275
276
277
278
279
280
281
282
283
284
285
286
287
288
289
290
291
292
293
294
295
296
297
298
299
300
301
302
303
304
305
306
307
308
309
310
311
312
313
314
315
316
317
318
319
320
321
322
323
324
325
326
327
328
329
330
331
332
333
334
335
336
337
338
339
340
341
342
343
344
345
346
347
348
349
350
351
352
353
354
355
356
357
358
359
360
361
362
363
364
365
366
367
368
369
370
371
372
373
374
375
376
377
378
379
380
381
382
383
384
385
386
387
388
389
390
391
392
393
394
395
396
397
398
399
400
401
402
403
404
405
406
407
408
409
410
411
412
413
414
415
416
417
418
419
420
421
422
423
424
425
426
427
428
429
430
431
432
433
434
435
436
437
438
439
440
441
442
443
444
445
446
447
448
449
450
451
452
453
454
455
456
457
458
459
460
461
462
463
464
465
466
467
468
469
470
471
472
473
474
475
476
477
478
479
480
481
482
483
484
485
486
487
488
489
490
491
492
493
494
495
496
497
498
499
500
501
502
503
504
505
506
507
508
509
510
511
512
513
514
515
516
517
518
519
520
521
522
523
524
525
526
527
528
529
530
531
532
533
534
535
536
537
538
539
540
541
542
543
544
545
546
547
548
549
550
551
552
553
554
555
556
557
558
559
560
561
562
563
564
565
566
567
568
569
570
571
572
573
574
575
576
577
578
579
580
581
582
583
584
585
586
587
588
589
590
591
592
593
594
595
596
597
598
599
600
601
602
603
604
605
606
607
608
609
610
611
612
613
614
615
616
617
618
619
620
621
622
623
624
625
626
627
628
629
630
631
632
633
634
635
636
637
638
639
640
641
642
643
644
645
646
647
648
649
650
651
652
653
654
655
656
657
658
659
660
661
662
663
664
665
666
667
668
669
670
671
672
673
674
675
676
677
678
679
680
681
682
683
684
685
686
687
688
689
690
691
692
693
694
695
696
697
698
699
700
701
702
703
704
705
706
707
708
709
710
711
712
713
714
715
716
717
718
719
720
721
722
723
724
725
726
727
728
729
730
731
732
733
734
735
736
737
738
739
740
741
742
743
744
745
746
747
748
749
750
751
752
753
754
755
756
757
758
759
760
761
762
763
764
765
766
767
768
769
770
771
772
773
774
775
776
777
778
779
780
781
782
783
784
785
786
787
788
789
790
791
792
793
794
795
796
797
798
799
800
801
802
803
804
805
806
807
808
809
810
811
812
813
814
815
816
817
818
819
820
821
822
823
824
825
826
827
828
829
830
831
832
833
834
835
836
837
838
839
840
841
842
843
844
845
846
847
848
849
850
851
852
853
854
855
856
857
858
859
860
861
862
863
864
865
866
867
868
869
870
871
872
873
874
875
876
877
878
879
880
881
882
883
884
885
886
887
888
889
890
891
892
893
894
895
896
897
898
899
900
901
902
903
904
905
906
907
908
909
910
911
912
913
914
915
916
917
918
919
920
921
922
923
924
925
926
927
928
929
930
931
932
933
934
935
936
937
938
939
940
941
942
943
944
945
946
947
948
949
950
951
952
953
954
955
956
957
958
959
960
961
962
963
964
965
966
967
968
969
970
971
972
973
974
975
976
977
978
979
980
981
982
983
984
985
986
987
988
989
990
991
992
993
994
995
996
997
998
999
1000

1 shown). Figure 5d shows renal pH map overlaid on a T_2 -weighted image. pH was found to be 7.0 ± 0.1 ,
2
3
4 6.8 ± 0.1 and 6.5 ± 0.2 for cortex, medulla and calyx, respectively, significantly different from each
5
6 other ($P < 0.05$). To demonstrate the advantage of the modified pH mapping, we investigated renal pH
7
8 from ratiometric analysis of the same RF power level at 4.7 T (e.g. ST(5.5 ppm)/ST(4.3 ppm) under 1.0
9
10 and 2.0 μT) and ST(5.5 ppm, 1.0 μT)/ST(4.3 ppm, 2.0 μT), all showing unsatisfactory results
11
12 (Supplementary Data). For example, ratiometric analysis of ST(5.5 ppm)/ST(4.3 ppm) under 1.0 μT
13
14 yielded underestimated renal pH of 6.4 ± 0.2 , 6.2 ± 0.3 and 5.8 ± 0.3 for cortex, medulla and calyx,
15
16 respectively (Supplementary Table 1). This suggests that the presence of pronounced concomitant MT
17
18 and direct saturation effects substantially confound in vivo pH determination using conventional
19
20 ratiometric analysis at sub-high/low field.
21
22
23
24
25
26

27 DISCUSSION

28 Our study generalized the routine ratiometric CEST analysis by mixing both RF power level and
29
30 chemical shift for the ratiometric analysis, further applied multi-pool Lorentzian model to resolve
31
32 overlapped CEST effects, and extended the range of pH detection at sub-high magnetic field. The
33
34 approach was applied to measure renal pH in vivo, providing pH quantification in good agreement with
35
36 prior findings at high field (2,19).
37
38
39
40

41 It has been shown that chemical exchange rate of iopamidol amide groups at 4.3 and 5.5 ppm
42
43 are both dominantly base-catalyzed, and the exchange rate at 5.5 ppm increases much more rapidly
44
45 with pH than that at 4.3 ppm (26). In addition, it has been well recognized that it takes higher RF
46
47 irradiation level to effectively saturate exchangeable groups undergoing faster chemical exchange.
48
49 Therefore, we extended the ratiometric pH imaging by ratioing CEST effects at mixed RF power levels
50
51 and offsets so that CEST effect at 5.5 ppm obtained under a higher RF power was normalized by CEST
52
53 effect at 4.3 ppm using a slightly lower RF power level. This is in contrast to prior ratiometric analysis
54
55 that ratios CEST effects at different chemical shifts obtained under the same saturation power or
56
57
58
59
60

1 compares CEST effects at the same chemical shift obtained under different saturation levels. The
2
3 proposed approach decoupled confounding concomitant saturation effects, therefore, provides robust
4
5 pH mapping. It helps to briefly discuss the selection of RF power levels for the modified ratiometric
6
7 analysis. Previous study shows that the contrast to noise of in vitro iopamidol pH imaging using the
8
9 conventional ratiometric pH analysis peaks for B_1 of 2.5 μT at 4.7 T (26). To account for more
10
11 pronounced concomitant MT and spillover effects in vivo, we reduced the B_1 level to 2.0 μT . A second
12
13 RF power level is needed for the generalized ratiometric pH analysis. We chose an intermediate RF
14
15 power level of 1 μT to balance between sufficient CEST effects without excessive broadening.
16
17
18
19
20

21 Our study found that renal pH gradually decreases from cortex, medulla to calyx, similar to
22
23 those obtained using pH-sensitive Gd-based contrast agent (1). The mean pH for the entire kidney was
24
25 6.9 ± 0.1 , comparable to that reported previously (2,19). By referencing the corresponding pH and
26
27 decoupled saturation transfer effects at 4.3 and 5.5 ppm from the phantom, averaged iopamidol
28
29 concentration estimated from the two saturation effects was 14.1 ± 5.0 , 16.9 ± 3.5 , and 20.9 ± 7.1 mM in
30
31 cortex, medulla and calyx, respectively. The normalized iopamidol concentration in cortex and
32
33 medulla with respect to that in the calyx was $67 \pm 7\%$ and $84 \pm 10\%$, respectively. The trend of normalized
34
35 iopamidol concentration significantly increased from cortex, medulla to calyx, consistent with the
36
37 known renal physiology.
38
39
40
41
42

43 It has been recognized that proper selection of initial guesses is critical for quantitative CEST
44
45 fitting, particularly for cases with suboptimal SNR, relatively large range of pH, and heterogeneous
46
47 contrast agent distribution. Our study here first increased SNR by down-sampling CEST-weighted
48
49 images, and the enhanced SNR and relaxed constraints warrant good estimation of fitting coefficients.
50
51 The fitting results determined under good SNR were used as initial guesses for the quantitative CEST
52
53 analysis, enabling semiautomatic and adaptive fitting per pixel. Notably, this approach allows using a
54
55
56
57
58
59
60

1
2 single set of initial guesses for the multi-pool Lorentzian model and fits all pixels in the kidney. Indeed,
3
4 good fitting performance was achieved for both phantom and in vivo kidney studies.
5
6
7

8 9 CONCLUSION

10
11 Our study generalized the conventional ratiometric CEST analysis, extended the iopamidol pH MRI
12
13 detection range, and further demonstrated renal pH in vivo at sub-high magnetic field.
14
15
16
17

18 19 ACKNOWLEDGEMENTS

20
21 This study was supported in part by National Natural Science Foundation of China (81571668), National
22
23 Basic Research Program of China (2015CB755500), Shenzhen Science and Technology Program
24
25 (GJHZ20160229200622417) and National Institute of Health (R01NS083654).
26
27
28
29
30
31
32
33
34
35
36
37
38
39
40
41
42
43
44
45
46
47
48
49
50
51
52
53
54
55
56
57
58
59
60

Figure Captions

Figure 1. Multi-pool Lorentzian decoupling of representative CEST Z-spectra from pH vial of 7.0, obtained under B_1 of (a) 1.0 μT and (b) 2.0 μT .

Figure 2. Extension of pH detection range using the modified ratiometric analysis (red circles) vs. that using the conventional simplistic ratiometric approach (blue squares).

Figure 3. Simplistic CESTR images (a) at 5.5 ppm acquired at 2.0 μT and (b) at 4.3 ppm obtained under 1.0 μT . (c) Ratiometric images show good pH sensitivity until pH of 7.0 (d). In comparison, (e) and (f) show CEST images obtained from the line-decoupling, with the modified ratiometric image shown in (g) that can capture pH as high as 7.5 (h).

Figure 4. Inverted Z-spectra measured at calyx (a, b), medulla (c, d), and cortex (e, f) from B_1 of 1.0 μT (left column) and 2.0 μT (right column) were fitted using a multi-pool Lorentzian model. ST effects at 5.5 ppm ($B_1=2.0 \mu\text{T}$, right column) decreases substantially from calyx (b), medulla (d), to cortex (f), while ST effect at 4.3 ppm ($B_1=1.0 \mu\text{T}$, left column) shows relatively small change (a, c, e).

Figure 5. Demonstration of renal pH map from a representative rat. The resolved maps of ST effects at (a) 5.5 and (b) 4.3 ppm were obtained with the decoupling method, from which (c) the modified ratiometric map was obtained. (d) pH map overlaid on corresponding T_2 -weighted image shows renal pH gradually decreases from the cortex, medulla to calyx.

References

1. Raghunand N, Howison C, Sherry AD, Zhang S, Gillies RJ. Renal and systemic pH imaging by contrast-enhanced MRI. *Magn Reson Med* 2003;49(2):249-257.
2. Longo DL, Busato A, Lanzardo S, Antico F, Aime S. Imaging the pH evolution of an acute kidney injury model by means of iopamidol, a MRI-CEST pH-responsive contrast agent. *Magn Reson Med* 2013;70(3):859-864.
3. Wang F, Kopylov D, Zu Z, Takahashi K, Wang S, Quarles CC, Gore JC, Harris RC, Takahashi T. Mapping murine diabetic kidney disease using chemical exchange saturation transfer MRI. *Magnetic Resonance in Medicine* 2016;76(5):1531-1541.
4. Stubbs M, Bhujwala ZM, Tozer GM, Rodrigues LM, Maxwell RJ, Morgan R, Howe FA, Griffiths JR. An assessment of ³¹P MRS as a method of measuring pH in rat tumours. *NMR Biomed* 1992;5(6):351-359.
5. van Sluis R, Bhujwala ZM, Raghunand N, Ballesteros P, Alvarez J, Cerdan S, Galons JP, Gillies RJ. In vivo imaging of extracellular pH using ¹H MRSI. *Magn Reson Med* 1999;41(4):743-750.
6. Garcia-Martin ML, Herigault G, Remy C, Farion R, Ballesteros P, Coles JA, Cerdan S, Ziegler A. Mapping extracellular pH in rat brain gliomas in vivo by ¹H magnetic resonance spectroscopic imaging: comparison with maps of metabolites. *Cancer Res* 2001;61(17):6524-6531.
7. Gallagher FA, Kettunen MI, Day SE, Hu DE, Ardenkjaer-Larsen JH, Zandt R, Jensen PR, Karlsson M, Golman K, Lerche MH, Brindle KM. Magnetic resonance imaging of pH in vivo using hyperpolarized ¹³C-labelled bicarbonate. *Nature* 2008;453(7197):940-943.
8. Alvarez-Pérez J, Ballesteros P, Cerdán S. Microscopic images of intraspheroidal pH by ¹H magnetic resonance chemical shift imaging of pH sensitive indicators. *Magnetic Resonance Materials in Physics, Biology and Medicine* 2005;18(6):293-301.
9. Zhang S, Wu K, Sherry AD. A Novel pH-Sensitive MRI Contrast Agent. *Angew Chem Int Ed Engl* 1999;38(21):3192-3194.
10. Garcia-Martin ML, Martinez GV, Raghunand N, Sherry AD, Zhang S, Gillies RJ. High resolution pH(e) imaging of rat glioma using pH-dependent relaxivity. *Magn Reson Med* 2006;55(2):309-315.
11. Beauregard DA, Parker D, Brindle KM. Relaxation-based mapping of tumor pH. 1998; Sydney, Australia. In: *Proceedings of the 6th Annual Meeting of ISMRM*. p 53.

12. Frullano L, Catana C, Benner T, Sherry AD, Caravan P. Bimodal MR-PET agent for quantitative pH imaging. *Angew Chem Int Ed Engl* 2010;49(13):2382-2384.
13. Aime S, Calabi L, Biondi L, De Miranda M, Ghelli S, Paleari L, Rebaudengo C, Terreno E. Iopamidol: Exploring the potential use of a well-established x-ray contrast agent for MRI. *Magn Reson Med* 2005;53(4):830-834.
14. Ward KM, Balaban RS. Determination of pH using water protons and chemical exchange dependent saturation transfer (CEST). *Magn Reson Med* 2000;44(5):799-802.
15. Wu R, Longo DL, Aime S, Sun PZ. Quantitative description of radiofrequency (RF) power-based ratiometric chemical exchange saturation transfer (CEST) pH imaging. *NMR Biomed* 2015;28(5):555-565.
16. Longo DL, Dastru W, Digilio G, Keupp J, Langereis S, Lanzardo S, Prestigio S, Steinbach O, Terreno E, Uggeri F, Aime S. Iopamidol as a responsive MRI-chemical exchange saturation transfer contrast agent for pH mapping of kidneys: In vivo studies in mice at 7 T. *Magn Reson Med* 2011;65(1):202-211.
17. Sheth VR, Liu G, Li Y, Pagel MD. Improved pH measurements with a single PARACEST MRI contrast agent. *Contrast Media Mol Imaging* 2010;7(1):26-34.
18. Moon BF, Jones KM, Chen LQ, Liu P, Randtke EA, Howison CM, Pagel MD. A comparison of iopromide and iopamidol, two acidoCEST MRI contrast media that measure tumor extracellular pH. *Contrast Media Mol Imaging* 2015;10(6):446-455.
19. Yang X, Song X, Banerjee SR, Li Y, Byun Y, Liu G, Bhujwala ZM, Pomper MG, McMahon MT. Developing imidazoles as CEST MRI pH sensors. *Contrast media & molecular imaging* 2016;11(4):304-312.
20. Wu Y, Zhang S, Soesbe TC, Yu J, Vinogradov E, Lenkinski RE, Sherry AD. pH imaging of mouse kidneys in vivo using a frequency-dependent paraCEST agent. *Magn Reson Med* 2016;75(6):2432-2441.
21. Longo DL, Sun PZ, Consolino L, Michelotti FC, Uggeri F, Aime S. A general MRI-CEST ratiometric approach for pH imaging: demonstration of in vivo pH mapping with iobitridol. *J Am Chem Soc* 2014;136(41):14333-14336.
22. Muller-Lutz A, Khalil N, Schmitt B, Jellus V, Pentang G, Oeltzschner G, Antoch G, Lanzman RS, Wittsack HJ. Pilot study of Iopamidol-based quantitative pH imaging on a clinical 3T MR scanner. *Magma* 2014;27(6):477-485.

- 1
2
3
4
5
6
7
8
9
10
11
12
13
14
15
16
17
18
19
20
21
22
23
24
25
26
27
28
29
30
31
32
33
34
35
36
37
38
39
40
41
42
43
44
45
46
47
48
49
50
51
52
53
54
55
56
57
58
59
60
23. Stancanello J, Terreno E, Castelli DD, Cabella C, Uggeri F, Aime S. Development and validation of a smoothing-splines-based correction method for improving the analysis of CEST-MR images. *Contrast Media Mol Imaging* 2008;3(4):136-149.
24. Kim M, Gillen J, Landman BA, Zhou J, van Zijl PCM. Water saturation shift referencing (WASSR) for chemical exchange saturation transfer (CEST) experiments. *Magn Reson Med* 2009;61(6):1441-1450.
25. Cai K, Singh A, Poptani H, Li W, Yang S, Lu Y, Hariharan H, Zhou XJ, Reddy R. CEST signal at 2ppm (CEST@2ppm) from Z-spectral fitting correlates with creatine distribution in brain tumor. *NMR Biomed* 2015;28(1):1-8.
26. Sun PZ, Longo DL, Hu W, Xiao G, Wu R. Quantification of iopamidol multi-site chemical exchange properties for ratiometric chemical exchange saturation transfer (CEST) imaging of pH. *Phys Med Biol* 2014;59(16):4493.
27. Zhou IY, Wang E, Cheung JS, Zhang X, Fulci G, Sun PZ. Quantitative chemical exchange saturation transfer (CEST) MRI of glioma using Image Downsampling Expedited Adaptive Least-squares (IDEAL) fitting. *Scientific Reports* 2017;7(1):84.

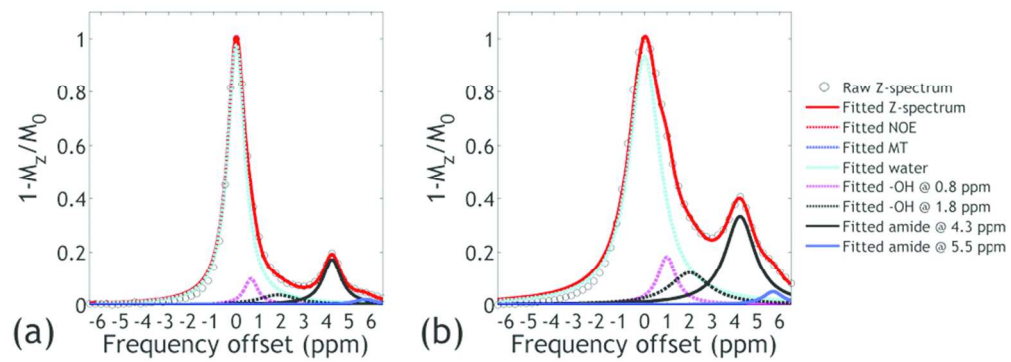


Figure 1. Multi-pool Lorentzian decoupling of representative CEST Z-spectra from pH vial of 7.0, obtained under B_1 of (a) $1.0 \mu\text{T}$ and (b) $2.0 \mu\text{T}$.

85x31mm (300 x 300 DPI)

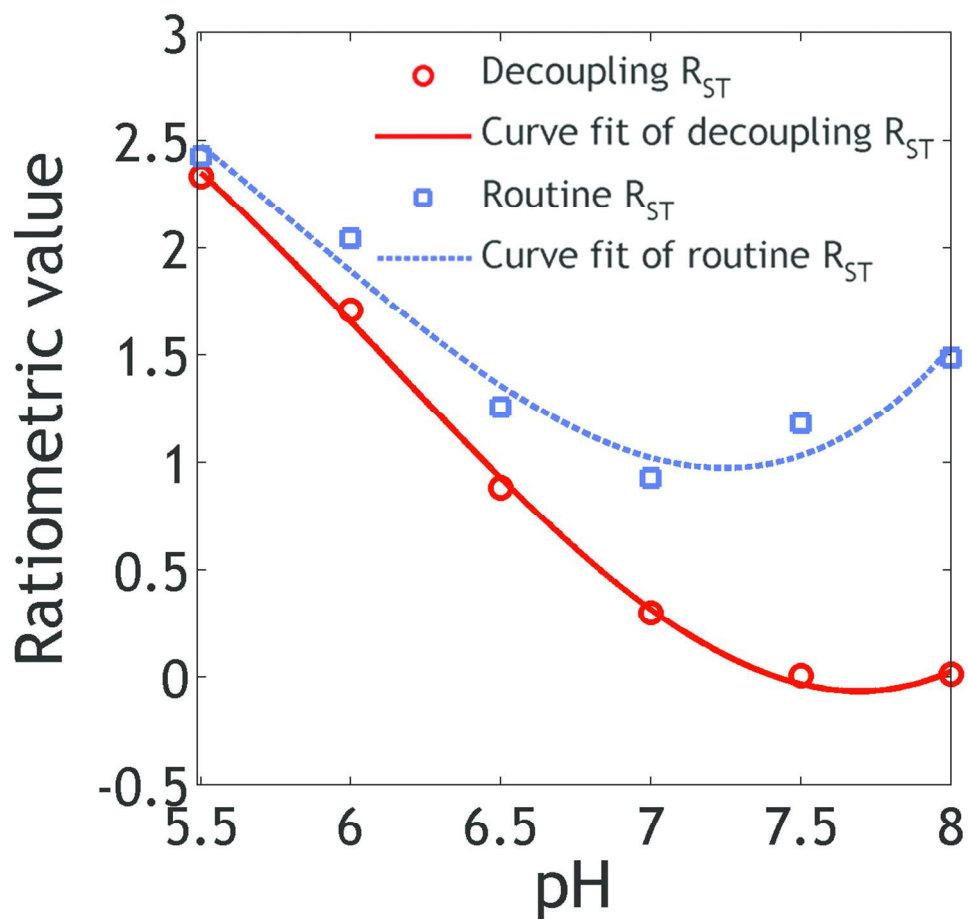


Figure 2. Extension of pH detection range using the modified ratiometric analysis (red circles) vs. that using the conventional simplistic ratiometric approach (blue squares).

115x106mm (300 x 300 DPI)



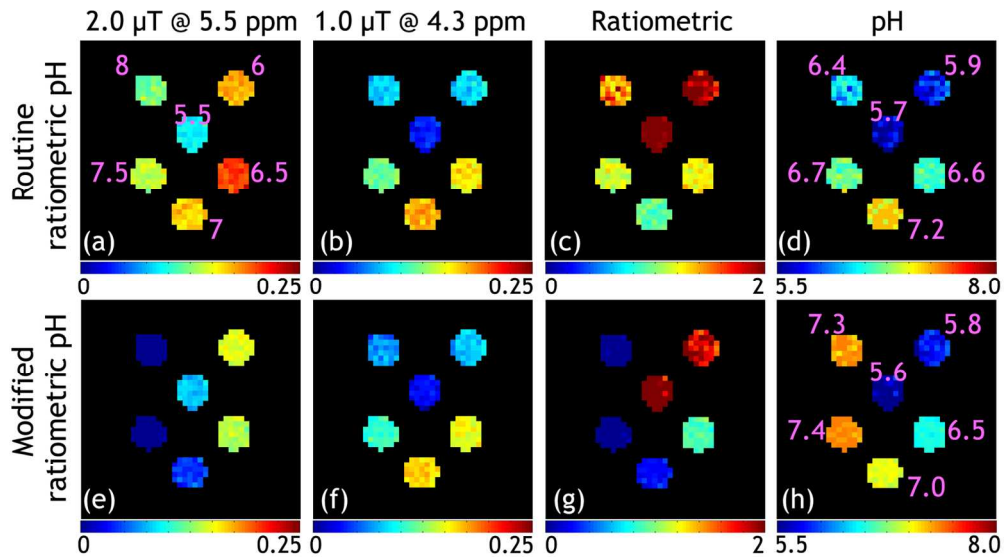


Figure 3. Simplistic CESTR images (a) at 5.5 ppm acquired at 2.0 μT and (b) at 4.3 ppm obtained under 1.0 μT . (c) Ratiometric images show good pH sensitivity until pH of 7.0 (d). In comparison, (e) and (f) show CEST images obtained from the line-decoupling, with the modified ratiometric image shown in (g) that can capture pH as high as 7.5 (h).

150x82mm (300 x 300 DPI)

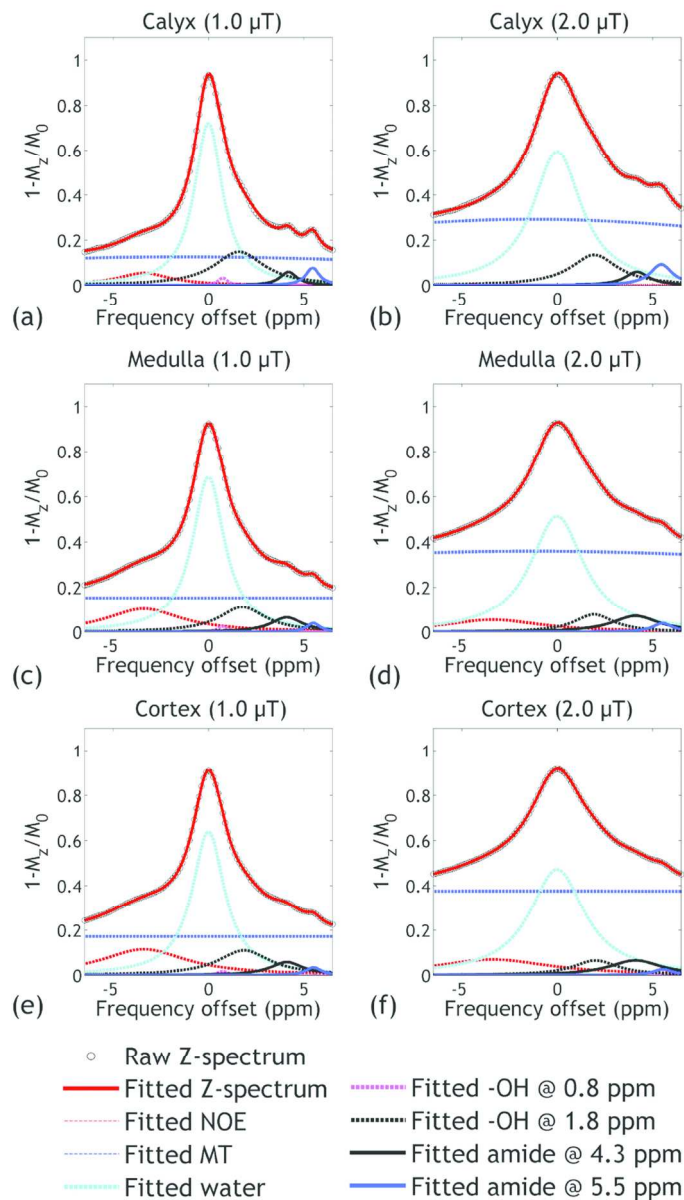


Figure 4. Inverted Z-spectra measured at calyx (a, b), medulla (c, d), and cortex (e, f) from B1 of 1.0 μT (left column) and 2.0 μT (right column) were fitted using a multi-pool Lorentzian model. ST effects at 5.5 ppm (B1=2.0 μT , right column) decreases substantially from calyx (b), medulla (d), to cortex (f), while ST effect at 4.3 ppm (B1=1.0 μT , left column) shows relatively small change (a, c, e).

85x151mm (300 x 300 DPI)

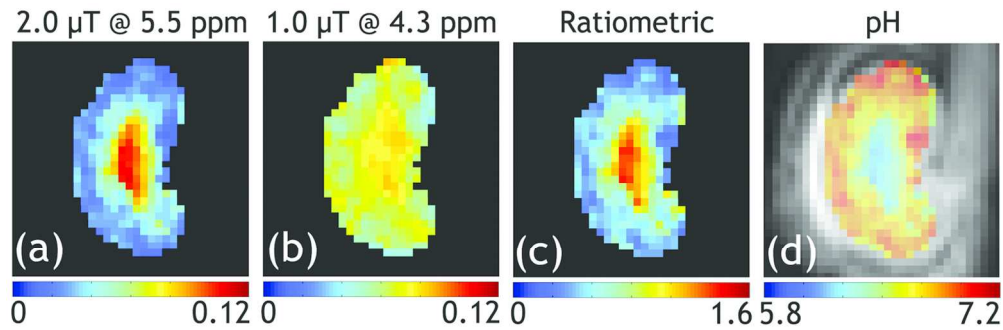


Figure 5. Demonstration of renal pH map from a representative rat. The resolved maps of ST effects at (a) 5.5 and (b) 4.3 ppm were obtained with the decoupling method, from which (c) the modified ratiometric map was obtained. (d) pH map overlaid on corresponding T2-weighted image shows renal pH gradually decreases from the cortex, medulla to calyx.

150x49mm (300 x 300 DPI)

SUPPLEMENTARY INFORMATION

A Generalized Ratiometric Chemical Exchange Saturation Transfer (CEST) MRI Approach for Mapping Renal pH using Iopamidol

Yin Wu, Iris Y. Zhou, Takahiro Igarashi, Dario L. Longo, Silvio Aime, and Phillip Zhe Sun

Data analysis

For the conventional non-decoupling methods, the ST effects at chemical shifts of 4.3 and 5.5 ppm were measured with asymmetric analysis of $ST(\omega) = \frac{M(-\omega) - M(\omega)}{M_0}$ where, ω is the chemical shift of iopamidol amide proton with respective water resonance, M_0 is signal intensity without RF irradiation. For the proposed decoupling methods, the ST effects at chemical shifts of 4.3 and 5.5 ppm were obtained by decoupling multi-pool CEST effects. Renal pH from ratiometric analysis of the same RF power level (e.g. $ST(5.5 \text{ ppm})/ST(4.3 \text{ ppm})$ under 1.0 and 2.0 μT) and mixed RF power levels (e.g. $ST(5.5 \text{ ppm}, 2.0 \mu\text{T})/ST(4.3 \text{ ppm}, 1.0 \mu\text{T})$) was investigated for both of the proposed and conventional ratiometric analysis methods, respectively.

FIGURE CAPTIONS

Figure S1. ST effects at (a) 5.5 ppm and (b) 4.3 ppm under the same saturation power of 1.0 μT were measured with the conventional non-decoupling method, from which (c) the ratiometric map was obtained. (d) pH map overlaid on a T2-weighted image shows that pH values of most of voxels in inner layers were less than 5.8, deviating from reported values.

Figure S2. ST effects at (a) 5.5 ppm and (b) 4.3 ppm under the same saturation power of 2.0 μT were measured with the conventional non-decoupling method, from which (c) the ratiometric map was obtained. (d) pH map overlaid on a T2-weighted image shows that the renal pH values are apparently underestimated compared to reported values.

Figure S3. ST effects at (a) 5.5 ppm ($B_1=2.0 \mu\text{T}$) and (b) 4.3 ppm ($B_1=1.0 \mu\text{T}$) were measured with the conventional non-decoupling method, from which (c) the ratiometric map was obtained. (d) pH map overlaid on a T2-weighted image shows that renal pH values at middle layers (<5.8) are smaller than those at calyx, inconsistent with reported values and renal pH pattern.

Table S1. Renal pH values measured by ratioing CEST effects at different chemical shifts of 5.5 and 4.3 ppm obtained under saturation powers of 1.0 and 2.0 μT with the conventional non-decoupling and proposed decoupling methods. Mean \pm standard deviation are presented.

		Cortex	Medulla	Calyx	Entire kidney
Non-decoupling method	1.0 μT	6.41 \pm 0.23	6.21 \pm 0.34	5.83 \pm 0.31	6.27 \pm 0.22
	2.0 μT	6.54 \pm 0.14	6.56 \pm 0.20	6.36 \pm 0.14	6.52 \pm 0.16
	2.0 μT /1.0 μT	6.32 \pm 0.31	6.05 \pm 0.22	5.93 \pm 0.20	6.19 \pm 0.23
Decoupling method	1.0 μT	6.31 \pm 0.23	6.28 \pm 0.14	5.95 \pm 0.28	6.26 \pm 0.21
	2.0 μT	6.66 \pm 0.17	6.61 \pm 0.11	6.44 \pm 0.16	6.61 \pm 0.14
	2.0 μT /1.0 μT	7.00 \pm 0.08	6.81 \pm 0.08	6.48 \pm 0.19	6.85 \pm 0.11

Figure S1.

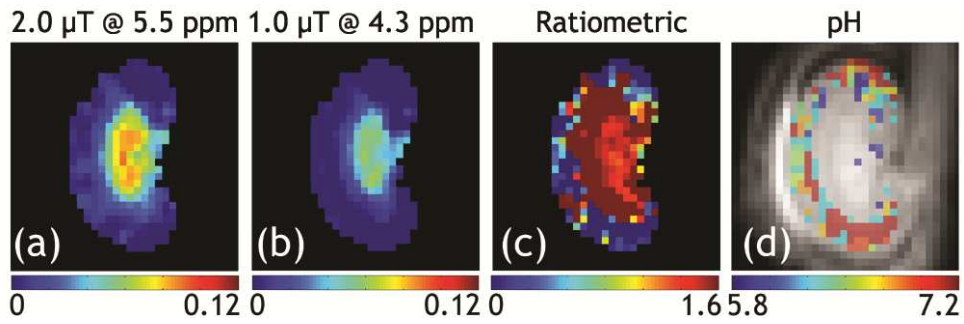


Figure S2.

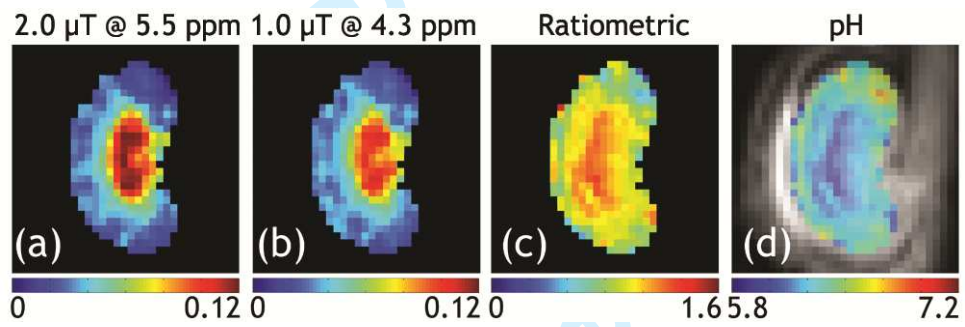


Figure S3.

